Copyright © 2007 by ABCM

INTERDROPLET SPACING EFFECTS DURING VAPORIZATION OF FUEL DROPLET STREAMS USING DISCRETE PHASE ENCAPSULATION

Guilherme Bastos Machado, **machadogb@petrobras.com.br**
Division of Engine Products
Petrobras Research Center
Albino José Kalab Leiroz, leiroz@mecanica.ufrj.br
Department of Mechanical Engineering – POLI/ COPPE
Universidade Federal do Rio de Janeiro

Abstract. *In the present paper the vaporization of isolated fuel droplets and linear arrays of fuel droplets in convective regime inside cylindrical ducts is studied under assumptions that allow comparisons with analytical solutions. The fuel droplets are positioned along the tube centerline allowing an axisymmetric analysis of the physical problem. For the gaseous phase, momentum, energy and species conservation equations are discretized using the Finite Difference Method. An implicit scheme is applied and the resulting system of algebraic equations is solved through iterative techniques with local error control. The discrete phase treatment makes use of vaporization models, avoiding numerical treatment of a non-regular domain. Laminar flow results are obtained for different number of droplets and interdroplet spacings. Limiting cases of isolated droplets and single-phase flows are used to validate and calibrate the developed numerical code. The analysis of the numerical results is focused on individual droplet vaporization rates, droplets interaction effects and heat transfer parameters along the solid contours.*

Keywords*: droplet vaporization, droplet-streams, laminar flow, entrance region, numerical methods*

1. INTRODUCTION

Liquid atomization and spray vaporization are used in a wide variety of industrial devices and processes. These applications include internal combustion and rocket engines, furnaces, heaters, humidification and misting processes, painting, and agricultural processes. The atomization process transforms a liquid stream passing through atomizers into dispersed liquid droplets immersed in a continuous gaseous phase. The atomization leads to an enhancement of energy and mass transfer processes between the continuous and discrete phases during spray vaporization and combustion. Sprays flows are characterized by the inherent coupling between the fluid dynamics and the transport of mass, momentum and energy between the phases on different length and time scales. These features lead to elaborate models and computationally intensive simulations. Investigations on the vaporization of isolated droplets and simple droplet arrays provide insight on the fundamental aspects of spray vaporization processes. Besides, these studies contribute to an improved understanding of the related physical phenomena and to the development of more precise spray vaporization models. Reviews on different aspects of droplet vaporization and combustion are found on Faeth (1977) and Sirignano (1999). For interaction studies, droplet-streams provide a simple and reproducible arrangement for numerical and experimental investigations (Castanet et al., 2005 and Orain et al., 2005).

Machado (2006) investigates the vaporization of isolated droplets and linear arrays of droplets in a continuous laminar and incompressible gaseous flow under isobaric conditions. A range of Reynolds number varying between 10 and 200 is considered. A simplified analysis of the coupling between the discrete and continuous phases is introduced and tested. A basis for the reduction of computational costs associated to numerical studies where a large number of droplets is considered is proposed. Fuel-air mixture distribution along the tube exit section is determined, including the fuel mass fraction average and standard deviation. The Nusselt number along the tube solid wall is also analyzed in order to verify the influence of droplet-stream presence on heat transfer parameters. The present paper extends the analyses investigating the influence of different interdroplet spacing on droplets interaction effects and vaporization rates.

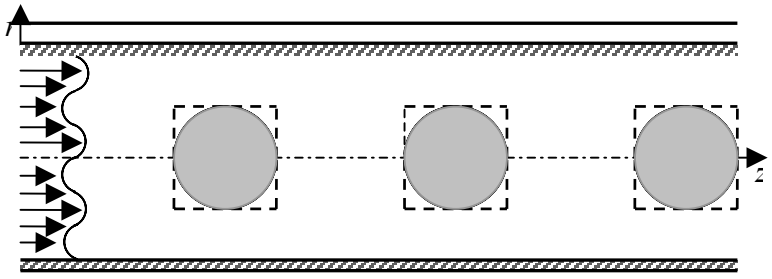

Figure 1. Scketch of the physical domain.

2. ANALYSIS

Figure 1 shows a sketch of the physical domain depicting a circular tube longitudinal section, fuel droplets and the cylindrical system of coordinates. Cylindrical capsules, marked by dashed lines in Fig.1, are used in modeling the droplet-flow interaction. The cylindrical capsules are used to represent the spherical droplets avoiding the treatment of the non-regular solution domain. Symmetry along the tube longitudinal axis allows a simplification of the solution domain. In the present work, energy and mass transfer between the fuel droplets and main air stream are studied, evaluating the convenience of the simplified approach for the vaporization of droplet-stream in laminar flows.

The two-dimensional and incompressible flow governing equations are written using a vorticity-stream function formulation, decoupling pressure from velocity calculations and automatically satisfying the continuity equation. The vorticity transport equation and the stream function Poisson-equation are written in non-dimensional form, respectively, as

$$\frac{\partial \xi}{\partial t} + u_r \frac{\partial \xi}{\partial r} + u_z \frac{\partial \xi}{\partial z} - \frac{u_r}{r}\xi = \frac{1}{Re}\left[\frac{\partial}{\partial r}\left(\frac{\xi}{r}\right) + \frac{\partial^2 \xi}{\partial r^2} + \frac{\partial^2 \xi}{\partial z^2}\right] \tag{1}$$

$$\frac{\partial^2 \psi}{\partial z^2} + r\frac{\partial}{\partial r}\left(\frac{1}{r}\frac{\partial \psi}{\partial r}\right) = -\xi r \tag{2}$$

Thermo-physical properties are assumed constant and body forces are considered negligible. Equations (1-2) are derived from the momentum conservation equations written in a cylindrical coordinate system using the vorticity and stream function definitions given in terms of velocity components, respectively, as

$$\xi = \frac{\partial u_r}{\partial z} - \frac{\partial u_z}{\partial r} \tag{3}$$

$$u_r = -\frac{1}{r}\frac{\partial \psi}{\partial z} \tag{4}$$

$$u_z = \frac{1}{r}\frac{\partial \psi}{\partial r} \tag{5}$$

The energy conservation equation is written in non-dimensional form in terms of temperature, assuming negligible radiation heat transfer and viscous dissipation effects, as

$$\frac{\partial T}{\partial t} + u_r \frac{\partial T}{\partial r} + u_z \frac{\partial T}{\partial z} = \frac{1}{Re\,Pr}\left[\frac{1}{r}\frac{\partial}{\partial r}\left(r\frac{\partial T}{\partial r}\right) + \frac{\partial^2 T}{\partial z^2}\right] \tag{6}$$

Assuming the fluid as a binary mixture of fuel vapor and air, a single chemical specie conservation equation is required to describe the mass fraction distribution. In the present work, the conservation of air, written as

$$\frac{\partial Y_a}{\partial t} + u_r \frac{\partial Y_a}{\partial r} + u_z \frac{\partial Y_a}{\partial z} = \frac{1}{Re\,Le\,Pr}\left[\frac{1}{r}\frac{\partial}{\partial r}\left(r\frac{\partial Y_a}{\partial r}\right) + \frac{\partial^2 Y_a}{\partial z^2}\right] \tag{7}$$

is used. The fuel mass fraction is obtained from

$$Y_a + Y_f = 1 \tag{8}$$

The non-dimensional variables used in Eq.(1-8) are defined using the tube radius r_0 and the maximum inlet velocity U_0 as the characteristic length and velocity as

$$r = \frac{r^*}{r_0},\ z = \frac{z^*}{r_0},\ u_r = \frac{u_r^*}{U_0},\ u_z = \frac{u_z^*}{U_0},\ \xi = \frac{\xi^* r_0}{U_0},\ \psi = \frac{\psi^*}{r_0^2 U_0},\ t = \frac{t^* U_0}{r_0},\ T = \frac{T_R^* - T^*}{T_R^* - T_e^*} \tag{9}$$

In Eq. (9), T_e^* and T_R^* are the inlet temperature and an arbitrarily chosen reference temperature, respectively. Reynolds, Prandtl and Lewis numbers are respectively defined as

$$Re = \frac{U_0 r_0}{\nu},\ Pr = \frac{\nu}{\alpha},\ Le = \frac{\alpha}{D} \tag{10}$$

For the liquid phase, infinite thermal conductivity model and negligible thermal inertia are assumed. Therefore, the droplet temperature is uniform and equal to the surface value. The quasi-steady assumption is also applied, avoiding the treatment of the droplet surface regression effects (Spalding, 1953). For the gaseous phase, thermo-physical properties are evaluated applying the 1/3-rule (Lefebvre, 1989).

The solution domain depicted in Fig.1 is non-regular, imposing limitations on the numerical methods applied for the phenomena analysis, which usually lead to the application of grid generation techniques. In the present work, an approximate procedure where the spherical droplets are encapsulated by cylindrical regions is proposed and tested.

Fully developed and isothermal flow ($T_e = 1$) of air ($Y_a = 1$) is considered at the tube inlet and the stream function distribution is obtained through integration of the velocity profile. Along the tube exit section, homogeneous flux boundary conditions are used implying fully developed profiles. Different tube lengths are tested in order to evaluate the assumption in finite solution domain.

Along the tube solid wall no-slip boundary conditions are applied to the axial velocity component leading to a constant stream function value equal to the volumetric flux per unit angle entering the tube. The wall temperature is specified at a different value of the entrance temperature ($T_w = 0$). The wall is impermeable to the mixture components and the species flux is set to zero. Therefore, the air mass fraction flux in the radial direction becomes equal to zero. At tube centerline, the symmetry conditions are used for the radial velocity, temperature and air mass fraction. Velocity symmetry leads to zero vorticity along the tube centerline. For convenience, the stream function value is chosen as zero along the tube centerline upstream of the leading droplet.

Vorticity values along tube inlet section and solid wall are not known. Vorticity values along the domain boundaries are obtained through an iterative procedure that makes use of a Taylor Series expansion of the stream function in a orthogonally to the specific boundary (Anderson et al., 1984).

In the present work, an approximated approach is used in specifying the boundary conditions at the droplet surface. In order to avoid the treatment of a non-regular domain, individual droplets are encapsulated within cylinders as shown in Fig.2. Along the encapsulating cylinder surface, appropriate boundary conditions are applied.

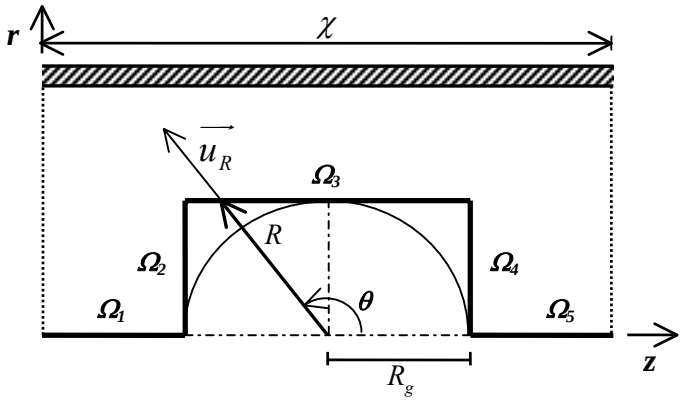

Figure 2 – Sketch of the Droplet Encapsulation.

It is assumed that all energy reaching the encapsulations is completely used for liquid vaporization. The droplet surface blowing velocity is a function of the temperature gradient at droplet surface and fuel latent heat of vaporization, Δh_v , as

$$u_R = \frac{k\left(T_e^* - T_R^*\right)}{\rho \Delta h_v r_0 U_0} \frac{\partial T}{\partial R}; \ \ (r,z) \in \Omega_2, \Omega_3, \Omega_4 \tag{11}$$

coupling the solutions of velocity and temperature fields. In Eq. (11), k and ρ are the mixture thermal conductivity and density, respectively.

The stream function values along the encapsulation boundary are determined through the numerical integration of the velocity components according to Eqs. (4-5). Within an interdroplet region, centerline stream function value remains constant and equal to calculated volumetric flow rate per unit angle of the upstream droplets. Vorticity along the encapsulation is calculated through the iterative procedure applied for the tube entrance and solid wall.

The air mass fraction along the droplet surface is determined from a mass balance at droplet surface and using Eq. (11) in order to consider the velocity compatibility as

$$\frac{\partial Y_f}{\partial R} = \frac{k\left(T_e^* - T_R^*\right)}{\rho D \Delta h_v}\left(Y_f - 1\right)\frac{\partial T}{\partial R}; \ \ (r,z) \in \Omega_2, \Omega_3, \Omega_4 \tag{12}$$

In the present work, insolubility of the air on the liquid phase is assumed (Spalding, 1953; Faeth, 1977). A relation between surface temperature and fuel mass fraction is obtained assuming thermodynamic equilibrium of ideal mixture, through the utilization of the Clausius-Clapeyron equation. The initial conditions, applied to all the solution domain interior points, are represented by Eq.(13) and correspond to the stagnant air at constant temperature.

$$u_z = 0;\ u_r = 0;\ \psi = 0;\ \xi = 0;\ T = T_0\ ;\ Y_a = 1;\ t = 0 \tag{13}$$

3. SOLUTION PROCEDURE

Droplet surface vaporization velocity, temperature and fuel mass fraction are functions of the main flow hydrodynamic and thermal conditions that are influenced by the droplet-stream. Therefore, an iterative solution procedure is necessary. The fuel vapor mass fraction along the droplet encapsulation is determined iteratively as a function of the temperature gradient at the spherical radius direction. A new temperature is determined as a function of the fuel vapor mass fraction through the Clausius-Clapeyron relation. The vaporization velocity at droplet encapsulation is calculated from the new temperature gradient. The governing equations are discretized using the Finite Difference Method. The resulting system of algebraic equations is solved simultaneously through Gauss Seidel with local relative error control. Computations are performed until the steady-state conditions are reached.

4. RESULTS

Initially, the developed numerical code was validated using test cases for limiting conditions. In the first test case, the droplets were removed and the solutions for an internal hydrodynamic developing flow for $Re = 20$ and 100 are compared to the numerical solutions available in the literature (Friedmann et al., 1968). A maximum deviation of 2.46% in the velocity field is observed. Temperature field solution is validated by comparing the obtained results for a hydrodynamic-developed and thermal-developing flow subjected to constant wall temperature, to the numerical results available from Schmidt and Zeldin (1970). For $Pe = 5$, a maximum deviation of 2.59% for the entrance region and 0.54% for the asymptotic value is observed for tube wall Nusselt number. For $Pe = 100$, the tube wall Nusselt number results are compared to the analytical solution (Kays and Crawford, 1980) for the Graetz problem, showing a maximum deviation of 11.88% for the entrance region and no deviation for the asymptotic value, within the precision of the calculations. The higher deviation for the entrance region is explained by the absence of axial conduction in the Graetz problem.

Table 1 – Vaporization Model Validation for $Re = 100$.

$\Delta\psi$	-0.00289962
$Q^*_{M_f}$	$6.90 \times 10^{-8}\ kg/s$
$Q^*_{M_{f\ conv}}$ - Faeth	$6.49 \times 10^{-8}\ kg/s$
ΔQ_{M_f} - Faeth	6.32%
$Q^*_{M_{f\ conv}}$ -Ranz Marshall	$6.90 \times 10^{-8}\ kg/s$
ΔQ_{M_f} - Ranz Marshall	0.00%

The droplet vaporization calculations are validated using an isolated n-heptane droplet positioned in a convective air stream for $Re = 1,\ 10,\ 100,\ 200$. The results are compared with analytical solutions available for isolated droplets vaporizing in stagnant environments (Spalding, 1953; Lefebvre, 1989). For validation purposes, the analytical solution is corrected by semi-empirical correlations in order to account for convective effects (Ranz and Marshall, 1952a, 1952b; Faeth, 1977). Similarly to Lefebvre (1989), a $200\mu m$ -diameter, n-heptane droplet in a stagnant environment at $773K$ with unitary Lewis number is considered. The thermo-physical properties were evaluated applying the 1/3-rule, leading to $Pr = 0.91$. For the droplet vaporization rate, the maximum deviation encountered using Ranz and Marshall correlation was 9.22% for $Re = 10$. Using the correlation proposed by Faeth (1977), the maximum deviation was 6.32% for $Re = 100$. Considering the droplet surface equilibrium temperature (T_g), and fuel mass fraction (Y_{f_g}), the maximum deviations observed were respectively 0.13% and 1.47%, for $Re = 10$. Results obtained for $Re = 100$ are shown in Tabs.1 and 2, where $\Delta\psi$ and $Q^*_{M_f}$ are, respectively, the calculated non-dimensional and dimensional droplet vaporization rate and $Q^*_{M_{f\ conv}}$ and ΔQ_{M_f} represent, respectively, the analytical solution corrected by semi-empirical correlations and the simulated to analytical solution percentage difference.

It is worth mentioning that for the validation cases using isolated droplets, the tube inlet and wall are at the same temperature, similarly to the conditions used in deriving the analytical solutions. Complete validation results are available from Machado (2005).

Table 2–Vaporization Model Validation for $Re = 100$.

$Re = 100$		*Lefebvre*	Δ [Lefeb.]
T_g	*0.08782*	-	-
T_g^*	*341.6K*	*341.8K*	*-0.06%*
Y_{f_g}	*0.680*	*0.679*	*0.15%*

.In order to evaluate the influence of interdroplet spacing on the droplets vaporization rates, a two droplet array vaporizing in a convective stream with $Re = 100$ is considered. Interdroplet spacings (χ) of two, three and four droplet diameters are considered. Unitary Lewis number and $Pr = 0.91$ are used in the numerical simulations, in order to allow for comparisons with isolated droplet results used for validation purposes. The value of the ratio between the droplet diameter to tube radius ratio is chosen as *0.1*. Further results showing the influence of the main flow convective effects on the droplets vaporization rates, on the droplets interaction effects and on the mixture characteristics at tube exit were discussed on Machado and Leiroz (2006).

Stream function details, temperature and fuel mass fraction fields for interdroplet distance equal of two diameters are shown in Figs.3-5, respectively. Droplet vaporization rates are presented in Table 3, which also includes the vaporization rate of an isolated droplet under similar conditions. The influence of droplet interaction effects is observed from the differences on the droplet vaporization rates when compared to the isolated droplet, as quantified by the $\Delta\psi$ values in Tab.3. Results indicate that the first droplet vaporization rate is *3.19%* lower than the vaporization rate observed for an isolated droplet under the similar conditions, showing the upstream droplet is weakly influenced by interference effects. The downstream droplet vaporization rate is *39.53%* lower than the leading droplet, showing stronger influence of droplet interaction effects. The leading droplet vaporization flux, associated to the main flow characteristics, promote the development of region of high fuel vapor concentration and lower temperature around the second droplet, which reduces temperature and fuel vapor mass fraction gradients at the liquid surface, leading to the reduction of vaporization rate.

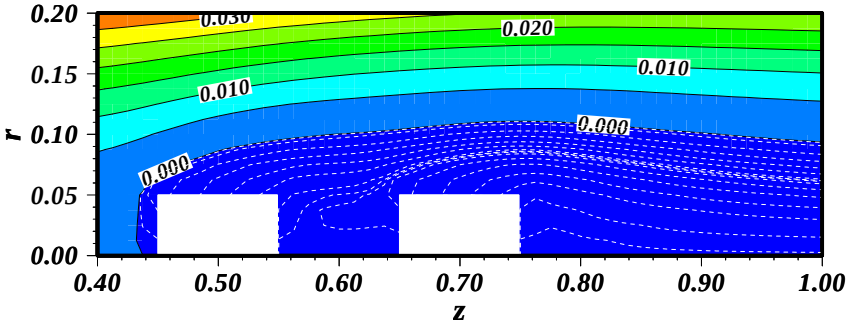

Figure 3 – Stream Function Field Details, case 1, $z_1 = 0.50$, $\chi = 2D_g$, $Re = 100$.

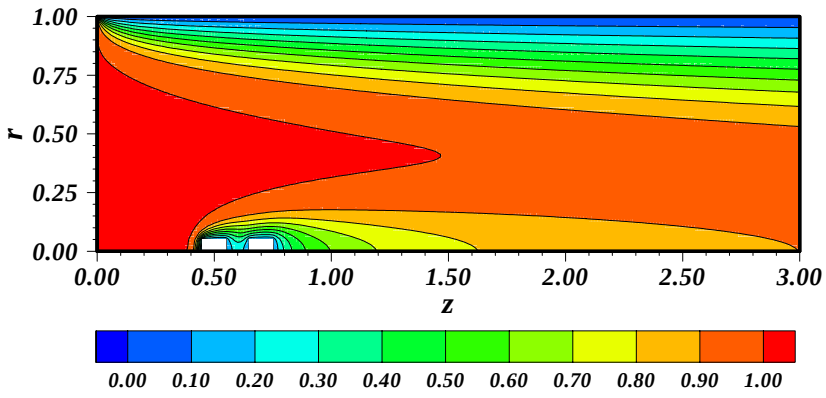

Figure 4 – Temperature Field, case 1, $z_1 = 0.50$, $\chi = 2D_g$, $Re = 100$.

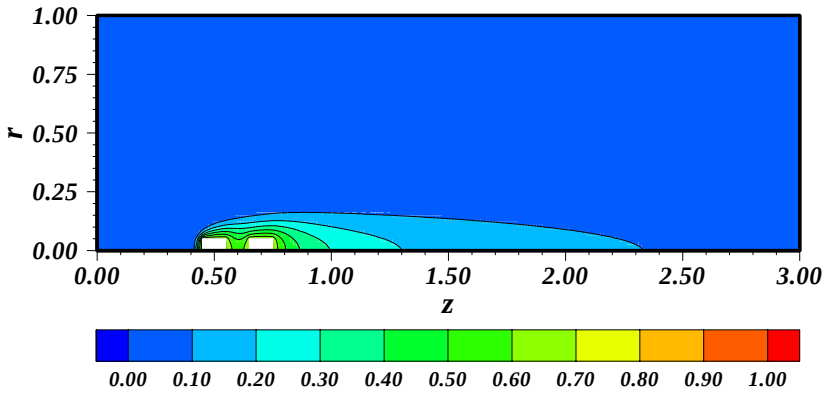

Figure 5 – Fuel Mass Fraction Field, case 1, $z_1 = 0.50$, $\chi = 2D_g$, $Re = 100$.

Table 3 – Droplet Vaporization Rates (*Isolated* and $\chi = 2D_g$).

$\Delta\psi$	*Isolated Droplet*	$\chi = 2D_g$
1^{st} *droplet*	*-0,00289962*	*-0,00280715*
2^{nd} *droplet*	-	*-0,00169745*

Results depicted in Figs.6-8 show stream function details, temperature and fuel mass fraction fields for an interdroplet spacing of three droplet diameters, respectively. Comparing the results shown in Figs.6-8 ($\chi = 3D_g$) and Figs.3-5 ($\chi = 2D_g$), variations on stream function, temperature and fuel mass fraction fields are observed. As the interdroplet spacing increases, streamlines emerging from the droplet surface are less influenced by the presence of the neighboring droplet. The development of recirculation zones in the interdroplet region is shown in Fig.6. For $\chi = 3D_g$, Figs.7-8 show a temperature increase and fuel mass fraction reduction on the interdroplet region, when compared to Figs.4-5, for $\chi = 2D_g$, which enhances liquid surface temperature and fuel mass fraction gradients. The droplet vaporization rates for $\chi = 3D_g$ are presented in Table 4. A less pronounced reduction of *1,48%* from the isolated conditions is observed for the upstream droplet vaporization rate. Results also show that the second droplet vaporization rate is *33,48%* inferior to that of the first droplet. It is observed that as interdroplet spacing increases from two to three droplet diameters an enhancement of individual droplet vaporization rates towards isolated droplet vaporization rate is observed. This behavior is justified by the reduction on droplet interference effects as the interdroplet spacing increases, as observed by the stream function, temperature and fuel mass fraction fields modifications.

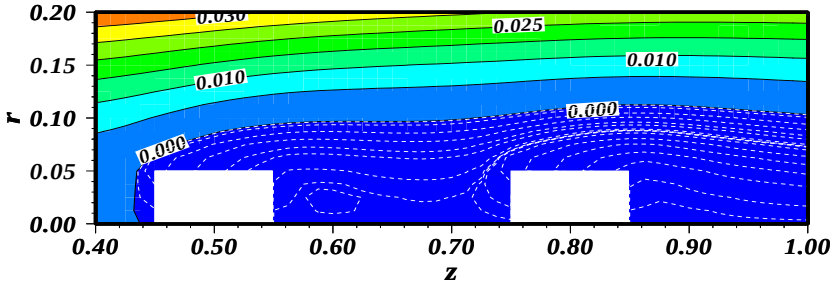

Figure 6 – Stream Function Field Details, case 2, $z_1 = 0.50$, $\chi = 3D_g$, $Re = 100$.

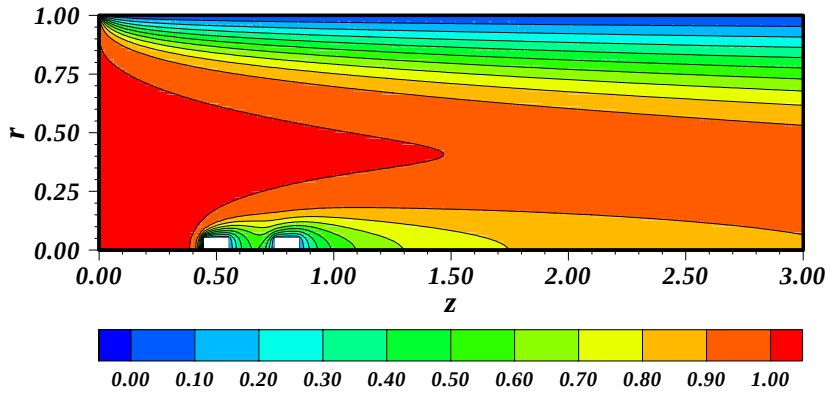

Figure 7 – Temperature Field, case 2, $z_1 = 0.50$, $\chi = 3D_g$, $Re = 100$.

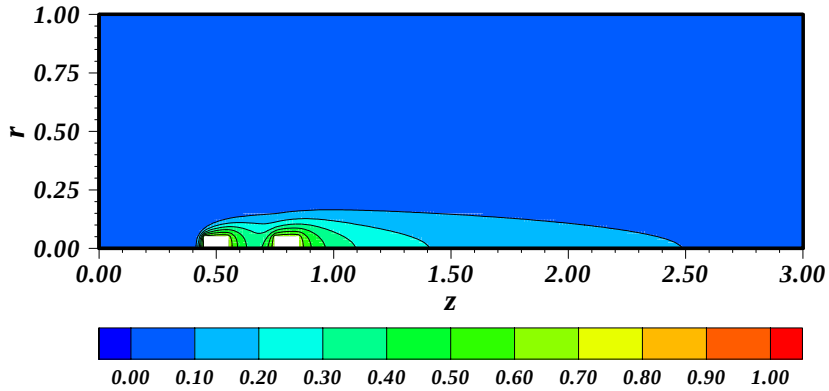

Figure 8 – Fuel Mass Fraction Field, case 2, $z_1 = 0.50$, $\chi = 3D_g$, $Re = 100$.

Table 4 – Droplet Vaporization Rates (*Isolated,* $\chi = 2D_g$ and $\chi = 3D_g$, $z_1 = 0.50$, $Re = 100$).

$\Delta\psi$	*Isolated Droplet*	$\chi = 2D_g$	$\chi = 3D_g$
1^{st} *droplet*	*-0,00289962*	*-0,00280715*	*-0,00285662*
2^{nd} *droplet*	-	*-0,00169745*	*-0,00190029*

Results depicted in Figs.9-11 show stream function details, temperature and fuel mass fraction fields for an interdroplet spacing of four diameters, respectively. Comparing the results shown on Figs.9-11 ($\chi = 4D_g$) and on Figs.6-8 ($\chi = 3D_g$), deviations on stream function, temperature and fuel mass fraction fields are observed. As the interdroplet spacing increases, streamlines originating on the droplets surface are less influenced by the presence of other droplet as shown in Figs.6 and 9. The recirculation zones within the interdroplet region are still present. For $\chi = 4D_g$, Figs.10-11 show further temperature increase and fuel mass fraction reduction within the interdroplet region, when compared to Figs.7-8 ($\chi = 3D_g$). Enhancements of liquid surface temperature and fuel mass fraction gradients are also observed. Individual droplet vaporization rates for $\chi = 4D_g$ are presented in Tab. 5. A less significant reduction of *0,89%* from the isolated condition is observed for the upstream droplet vaporization rate. Results also show that the second droplet vaporization rate is *29,17%* inferior to that of the first droplet showing that the reduction on droplet interference effects as the interdroplet distance is increased, as observed by the stream function, temperature and fuel mass fraction fields modifications.

In order to study the solid tube wall influence on the droplet vaporization rates, results were obtained using the same tube wall thermal boundary condition as in validation, $T_w = 1$. No observable variation on droplet vaporization rates is observed. Therefore, for the Reynolds number considered for the simulations, the differences observed on droplets vaporization rates are associated with droplet interaction effects. Besides, results also show no influence of the tube wall on the droplets vaporization rates for the conditions considered. Nevertheless, as can be seen on Machado and Leiroz (2006), for $Re = 10$, the less intensive convective effects associated to the wall boundary condition contributes to a higher difference between the leading droplet and an isolated droplet vaporization rates. Besides, influence on the downstream droplet vaporization rate is also observed in Machado nd Leiroz (2006) for lower Reynolds conditions.

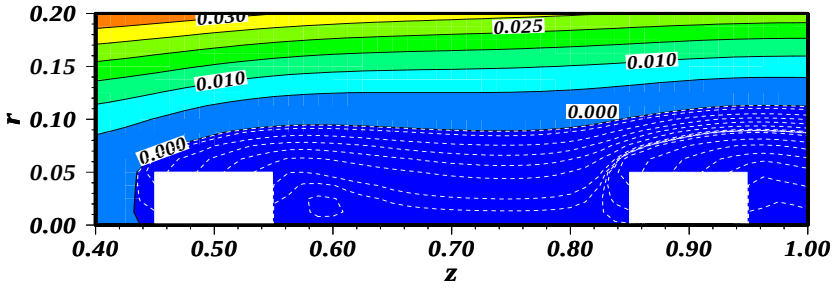

Figure 9 – Stream Function Field Details, case 3, $z_1 = 0.50$, $\chi = 4D_g$, $Re = 100$.

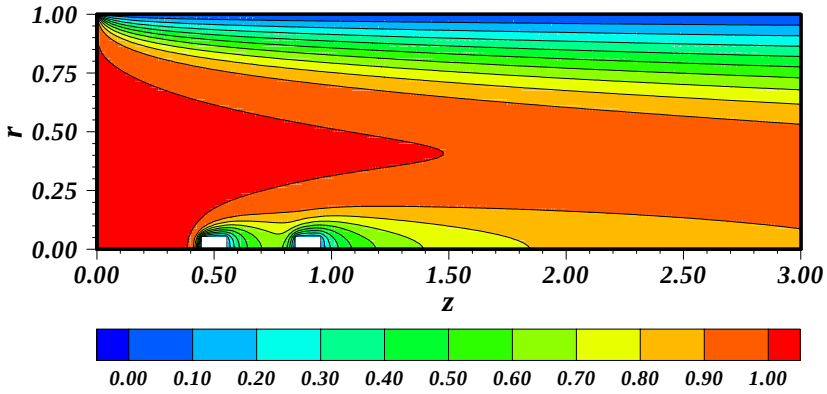

Figure 10 – Temperature Field, case 3, $z_1 = 0.50$, $\chi = 4D_g$, $Re = 100$.

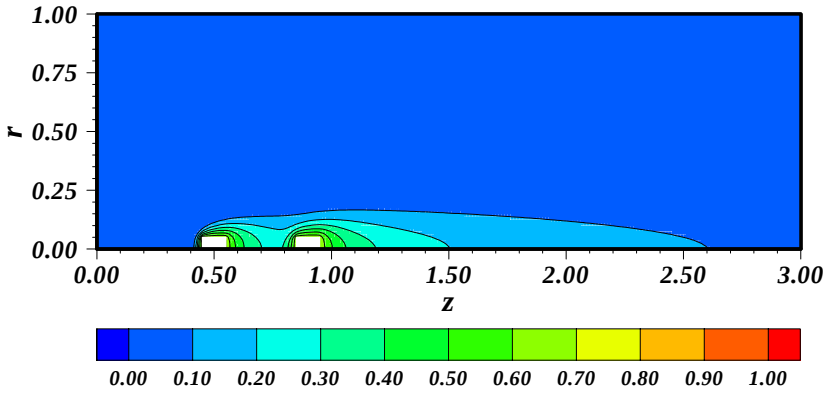

Figure 11 – Fuel Mass Fraction Field, case 3, $z_1 = 0.50$, $\chi = 4D_g$, $Re = 100$.

Table 5 – Droplet Vaporization Rates (*Isolated,* $\chi = 2D_g$, $\chi = 3D_g$ and $\chi = 4D_g$, $z_1 = 0.50$, $Re = 100$).

$\Delta\psi$	*Isolated Droplet*	$\chi = 2D_g$	$\chi = 3D_g$	$\chi = 4D_g$
1st droplet	*-0,00289962*	*-0,00280715*	*-0,00285662*	*-0,00287367*
2nd droplet	-	*-0,00169745*	*-0,00190029*	*-0,00203538*

Droplet-stream influence on the tube wall Nusselt number for the different spacings considered in the present work is shown in Fig.12. For $\chi = 2D_g$, a Nusselt number increase of *3.05%* is observed at $z = 0.80$, when compared to droplet-free value. For $\chi = 3D_g$ and $\chi = 4D_g$, the Nusselt number increases, respectively, by *3.04%* and *2.77%* in relation to the results where no droplets are present at $z = 0.80$. The *Nu* increase when a droplet-stream presence is explained by a decrease in the average mixture temperature in the radial section as well as by an increase in the wall temperature gradient in the radial direction.

5. CONCLUSIONS

The present work investigates the vaporization of linear arrays of fuel droplets under convective conditions within the entrance region of cylindrical ducts. The droplet-streams were positioned along the tube centerline in order to allow for an axisymmetric analysis of the physical phenomena. The discrete phase was treated applying vaporization models and avoiding numerical treatment of a non-regular domain. Results were obtained for laminar flow, $Re = 100$, with variable interdroplet spacing. Limiting cases of single-phase flow and isolated droplet vaporization were used for validation and calibration of the developed numerical procedure. The simplified approach of encapsulating the droplets showed the same order of magnitude than the simplifications present on analytical calculations, corrected by semi-empirical correlations existent on the literature. Individual droplet vaporization rates are obtained from the numerical solution, allowing for the quantification of the droplet interference effects. The droplet-stream influence on heat transfer parameters on the tube solid contours is also evaluated. For the laminar regime and the range of interdroplet distances considered the vaporization interaction effects and the influence of droplets presence on heat transfer parameters showed to be strong. The developed numerical code has the flexibility to simulate variable entrance conditions, tube lengths and variable number of droplets equally spaced, limited only by computational costs.

Copyright © 2007 by ABCM

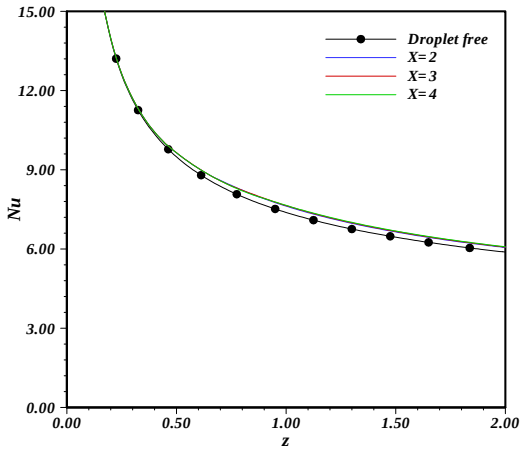

Figure 12 – Tube Wall Nusselt Number, with and without droplets
($\chi = 2D_g$, $\chi = 3D_g$, $\chi = 4D_g$), $z_l = 0.50$, $Re = 100$.

6. ACKNOWLEDGEMENTS

The authors acknowledge the financial support allocated by CAPES, CNPq and FAPERJ. Computer resources were allocated by the Thermal Engines Laboratory of the Federal University of Rio de Janeiro.

7. REFERENCES

Anderson, D. A., Tannehill, J. C. and Pletcher, R. H., 1984, Computational Fluid Mechanics and Heat Transfer. New York, Hemisphere Publishing Corporation;

Castanet, G., Lebouché, M. and Lemoine, F., 2005, Heat and Mass Transfer of Combusting Monodisperse Droplets in a Linear Stream, International Journal of Heat and Mass Transfer, v. 48, pp. 3261-3275;

Faeth, G. M., 1977, Current Status of Droplet and Liquid Combustion, Progress in Energy and Combustion Science, v. 3, pp. 191-224;

Friedmann, M., Gillis, J. and Liron, N., 1968, Laminar Flow in a Pipe at Low and Moderate Reynolds Numbers, Applied Scientific Research, v. 19, pp. 426-438;

Kays, W. M. and Crawford, M. E., 1980, Convective Heat and Mass Transfer. 2 ed. USA, McGraw-Hill;

Labowsky, M., 1976, The Effects of Nearest Neighbor Interactions on the Evaporation Rate of Cloud Particles, Chemical Engineering Science, v. 31, pp. 803-813;

Lefebvre, A. H., 1989, Atomization and Sprays, Washington D. C., Hemisphere Publishing Corporation;

Machado, G., B., 2005, Droplet Stream Vaporization in Circular Ducts Using Discrete Phase Encapsulation, M.Sc. Dissertation, COPPE, Universidade Federal do Rio de Janeiro, R.J., Brazil, *in Portuguese*;

Machado, G. B. and Leiroz, A. J. K., 2006, Droplet Stream Interference Effects in the Thermal and Hydrodynamic Entrance Region of Circular Ducts, In: Proceedings of the 13th International Heat Transfer Conference, Sydney, Austrália;

Orain, M., Mercier, X. and Grisch, F., 2005, PLIF Imaging of Fuel-Vapor Spatial Distribution Around a Monodisperse Stream of Acetone Droplets: Comparison with Modeling, Combustion Science and Technology, v. 177, pp. 249-278;

Ranz, W. E., and Marshall, W. R., 1952a, Evaporation from Drops – Part I", Chem. Eng. Progress, v. 48, pp. 141-146;

Ranz, W. E. and Marshall, W. R., 1952b, Evaporation from Drops – Part II, Chem. Eng. Progress, v. 48, pp. 173-180;

Schmidt, F. W. and Zeldin, B., 1970, Laminar Heat Transfer in the Entrance Region of Ducts, Applied Scientific Research, v. 23, pp. 73-94;

Sirignano, W. A., 1999, Fluid Dynamics and Transport of Droplets and Sprays, Cambridge University Press;

Spalding, D. B., 1953, The Combustion of Liquid Fuels. In: Proceedings of the Forth International Symposium on Combustion, pp. 847-864, Baltimore, MD.